Lightning NO_x Emissions: Reconciling measured and modeled estimates with updated NO_x chemistry

B. A. Nault,[1,a] J. L. Laughner,[2] P. J. Wooldridge,[2] J. D. Crounse,[3] J. Dibb,[4] G. Diskin,[5] J. Peischl,[6,7] J. R. Podolske[8], I. B. Pollack,[6,7,b] T. B. Ryerson,[6] E. Scheuer,[4] P. O. Wennberg[3,9], R. C. Cohen[1,2,]*

1. Department of Earth and Planetary Science, University of California, Berkeley, California, USA

2. Department of Chemistry, University of California, Berkeley, California, USA

3. Division of Geological and Planetary Sciences, California Institute of Technology, Pasadena, California, USA

4. Earth Systems Research Center, Institute for the Study of Earth Oceans and Space, University of New Hampshire, Durham, New Hampshire, USA

5. NASA Langley Research Center, Hampton, Virginia, USA

6. Chemical Sciences Division, Earth System Research Lab, National Oceanic and Atmospheric Administration, Boulder, Colorado, USA

7. Cooperative Institute for Research in the Environmental Sciences, University of Colorado, Boulder, Boulder, Colorado, USA

8. NASA Ames Research Center, Mountain View, California, USA

9. Division of Engineering and Applied Science, California Institute of Technology, Pasadena, California, USA

a. Now at Cooperative Institute for Research in the Environmental Sciences and Department of Chemistry, University of Colorado, Boulder, Colorado, USA

b. Now at Atmospheric Science Department, Colorado State University, Fort Collins, Colorado, USA

** Corresponding Author: Phone: (510)-642-2735. E-mail: rccohen@berkeley.edu*

Contents of this file

- Description of observations and model
- Tables S1 – S4.
- Figures S1 – S9.

.

DC-8 In Situ Observations during DC3

The observations [*Archive*] used in this study include NO and O_3 from chemilumiscence [*Ryerson et al.*, 1999], NO_2 from laser-induced fluorescence [*Thornton et al.*, 2000; *Nault et al.*, 2015], HNO_3 from mist chamber-ion chromatography [*Talbot et al.*, 1997] and chemical ionization-mass spectrometry [*Crounse et al.*, 2006], water vapor from diode laser hygrometer [*Diskin et al.*, 2002], and methyl peroxy nitrate and ΣANs from thermal-dissociation laser-induced fluorescence [*Day et al.*, 2002; *Nault et al.*, 2015]. We took the average of the two HNO_3 measurements for this study since there was a 10% difference between the two measurements [*Nault et al.*, 2016].

The observations used to compare to the GEOS-Chem simulated values were constrained between 200 and 350 hPa with O_3/CO less than 1.5 (removes stratospheric influences) [*Hudman et al.*, 2007]. A minimum of 10 1-minute averaged observations are required to ensure enough spatial coverage of the 2°×2.5° grid cell. Only observations with a NO_x/HNO_3 ratio less than 5 were used since higher ratios are associated with the near-field of convective emissions and the large model grid cell size dilutes fresh lightning NO_x emissions [*Bertram et al.*, 2007; *Henderson*

et al., 2011; *Cooper et al.*, 2014]. During DC3, 70% of upper tropospheric (P = 200–350 hPa) observations had NO_x/HNO_3 ratios less than 5. A sensitivity analysis on this ratio is discussed below, and, in general, the ratio does not impact the results of this study.

Airborne, in situ observations of NO_2 or NO_x, in the upper troposphere (T < 250 K), are prone to positive biases due to the thermal decomposition of methyl peroxy nitrate ($CH_3O_2NO_2$) and pernitric acid (HO_2NO_2) [*Browne et al.*, 2011; *Nault et al.*, 2015]. Depending on the residence time of the instrument and amount of $CH_3O_2NO_2$ and HO_2NO_2 in the air, the thermally decomposed $CH_3O_2NO_2$ and HO_2NO_2 can lead to a 10 – 50% positive bias for the in situ NO_2 measurements [*Nault et al.*, 2015]. Browne et al. [2011] estimated for aged air (e.g., far-field lightning NO_x studies), the in situ TD-LIF NO_2 measurements (prior to DC3) were ~35% too high due to the thermal decomposition of these species. Results from prior far-field measurements using TD-LIF measurements [e.g., *Hudman et al.*, 2007; *Martini et al.*, 2011] are therefore corrected by reducing NO_2 by ~35%. Interference in the TD-LIF NO_2 measurements during DC3 used in this work has been corrected as discussed by Nault et al. [2015]. The impacts of the thermal decomposition of these species on near-field, in situ measurements of NO_x referenced in this work are discussed in detail in Sect. 3.2.

OMI NO_2 Data Descriptions

The Ozone Monitoring Instrument (OMI) aboard the NASA Aura satellite is a UV/Vis spectrometer observing solar irradiance and sunlight reflected from Earth's surface in the 270 – 500 nm wavelength range [*Levelt et al.*, 2006]. The instrument, with a field of view of 2600 km swath with a ground pixel size between 13×24 km^2 at nadir to approximately 24×128 km^2 at the

edge of the swath, achieves near global coverage daily with an overpass time at approximately 13:40 local time.

We use observations from OMI to constrain global lightning NO_x emissions by comparing to GEOS-Chem columns at the regional scale. To match both the NASA Standard Product (v2.1) and the DOMINO product (v2) to GEOS-Chem grid cells, observations are first filtered for the presence of clouds and the effects of the row anomaly. Pixels with a geometric cloud fraction greater than 30% are removed. The row anomaly is an obstruction that affects the observed radiances of ~20 rows of pixels on the OMI instrument. The affected pixels are flagged in both products and are removed. The DOMINO user manual (http://www.temis.nl/docs/OMI_NO2_HE5_2.0_2011.pdf) indicates that pixels with a surface albedo >0.3 should be removed; we implement this criterion for both products for consistency. Because only SP v2 provides a daily gridded product, we begin with the ungridded Level 2 product for both SP v2 and DOMINO and match them to GEOS-Chem grid cells directly. Pixels are matched to GEOS-Chem grid cells if the pixel center falls within the grid cell, and a weighted average of all such observations is taken to produce a superobservation for comparison with the modeled NO_2 column. The weight used is that described in the OMNO2d readme (https://disc.sci.gsfc.nasa.gov/Aura/data-holdings/OMI/documents/v003/OMNO2_readme_v003.pdf):

$$w_{ij} = \left(1 - \frac{A_i - A_{min}}{A_{max}}\right) \times \left(\frac{A_{ij}}{A_j}\right) \qquad \text{Equation 1}$$

where w_{ij} is the weight that pixel i contributes to the average in grid cell j. A_i is the pixel area, A_{min} the minimum pixel size, A_{max} the maximum pixel size, A_{ij} the area that pixel i and grid cell j overlap, and A_j the area of the grid cell. For the SP, the averaging kernels are calculated as the given scattering weights divided by the tropospheric AMF. For DOMINO, the given averaging

kernels are converted from total-column to tropospheric by multiplying by the ratio of the total over tropospheric AMFs [Boersma et al. 2011]. The weighted average of all averaging kernels for these pixels is applied to the modeled NO_2 profile before calculating the modeled NO_2 column to remove the influence of the *a priori* profiles. The regional temporal average and standard deviation of the model-satellite difference weights each satellite superobservation-model grid cell pair by the total of all the individual weights within the superobservation.

To address possible biases in the GEOS-Chem NO_2:NO_x ratios, we calculate model columns with as-is GEOS-Chem NO_2 profiles and profiles scaled by the ratio $r_{DC3}/r_{GEOS\text{-}Chem}$, where r is the NO_2:NO_x ratio. To scale the GEOS-Chem profiles, the ratios in Figure S7 are interpolated to the model NO_2 profile pressure levels before multiplying each model level of the profile by the corresponding $r_{DC3}/r_{GEOS\text{-}Chem}$. For pressures where $r_{GEOS\text{-}Chem}$ is available but r_{DC3} is not, the nearest value of r_{DC3} is used. For pressures where neither r is available, both r_{DC3} and $r_{GEOS\text{-}Chem}$ are set to 1. The GEOS-Chem NO_2:NO_x ratios were averaged over the entire DC3 domain for this calculation.

GEOS-Chem Description

We evaluated the model by comparison to observations from in situ and space-based platforms. For the case with optimized kinetics compared to observations, we assessed a range of lightning NO_x parameters to find those that adequately represent the NO_x and HNO_3 observations. Simulations were allowed to spin-up from January 2011 to December 2011, and the 2012 calendar year was used for analysis. The simulated fields were averaged between 12:00 – 14:00 local standard time for comparison to satellite observations from the Ozone Monitoring Instrument (OMI) [*Levelt et al.*, 2006] and 16:00 – 20:00 local standard time for comparison with in situ observations [*Barth et al.*, 2015].

We integrate simulated NO_2 mixing ratios from the surface to modeled tropopause to compare to OMI NO_2 tropospheric columns. The AMF formulation given in the OMNO2 Theoretical Basis document [*Boersma et al.*, 2002], which is – to the best of our knowledge – used in both the NASA SPv2 and DOMINO retrievals, includes a multiplicative correction for below-cloud NO_2. Therefore, we compare modeled and satellite-observed tropospheric columns without adjusting the modeled columns to remove below-cloud NO_2.

We compare GEOS-Chem output to measurements of NO_x, HNO_3, O_3, H_2O, and sum of alkyl and multifunctional nitrates (ΣANs) mixing ratios between 200 and 350 hPa from the Deep Convective Clouds and Chemistry (DC3) campaign. Only GEOS-Chem grid cells that contained a minimum of 10 1-minute observations on that date were used in the comparison with the DC3 observations. For the comparisons in Figures 3, S4, S5, and S6, an unweighted average of all DC3 observations that lie within these grid cells is compared to an unweighted averaged of these GEOS-Chem grid cells.

To minimize the influence of surface NO_x sources (soil, anthropogenic, and biomass burning), which cannot be easily separated from lightning NO_x emissions using a tropospheric column nadir satellite observation, we focused on regions where the model predicts the lightning NO emissions are more than 60% of the NO_x source, similar to prior studies [e.g., *Martin et al.*, 2007]. Observations over South America, Northern Africa, Southern Africa, and Southeast Asia (Table S2 of the supporting information) during their summer months met this criterion.

Description of Calculations for Supplemental Figure 4

As stated in Section 3.1, it was calculated in Nault et al. [2016] that the UT NO_x lifetime is ~3 hrs in the first 6 hours of chemical aging, and after the 6 hours, the lifetime increases to ~0.5 – 1.5 days. For the simplified calculations in Figure S4, we assume a NO_x lifetime of 3

hours for the first 6 hours of photochemistry; then, we increase it to 1 day for the remaining photochemistry. We initialize the simplified calculation with the average NO_x calculated in Figure 1b (1200 pptv), and we use Eq. 1 from Section 3.2. The NO_x is either released at 07:00 (morning emission) or 17:00 (afternoon emission) local time, representative of the observations during DC3 [*Barth et al.*, 2015; *Pollack et al.*, 2016]. Finally, we assume 12 hours of sunlight, from 07:00 – 19:00 local time, with minimal loss of NO_x during nighttime, as shown in the N_2O_5 sensitivity runs (Figure S2b). During times of OMI overpass times, the simplified calculation shows that the NO_x from lightning emissions is still enhanced above the average UT NO_x background from DC3 of ~100 pptv [*Barth et al.*, 2015].

Sensitivity Analysis on the NO_x/HNO_3 Filtering Ratio on This Study

We used a NO_x/HNO_3 ratio < 5 in this study to filter the DC3 observations to compare with the GEOS-Chem simulations, to account for dilution of fresh lightning NO_x emissions that are not well captured in the model [*Bertram et al.*, 2007; *Henderson et al.*, 2011; *Cooper et al.*, 2014]. In Supplemental Table 3, we investigated the simulations-to-observations comparisons with different NO_x/HNO_3 ratios (5, 10, and all data). In general, the simulated NO_x is too low compared to observations and show that the lightning NO_x emissions should be increased. The overestimation of the simulated HNO_3 compared to the observed HNO_3 increases as the NO_x/HNO_3 ratio increases, further showing the impact of dilution of the thunderstorms in the GEOS-Chem grid. Similar to the NO_x sensitivity, the HNO_3 sensitivity results indicate that improving the UT NO_x chemistry provides the ability to increase the lightning NO_x emission rates to improve the simulated-to-observed UT NO_x during DC3.

Supplemental Table 1. Description of the different chemical cases investigated in this study. The MPN case is the standard chemistry found in GEOS-Chem v9-02.

Case Name	Description
Base case	Sander et al. [*Sander et al.*, 2011] recommended gas-phase rate constants, Evans and Jacob [*Evans and Jacob*, 2005] recommended N_2O_5 hydrolysis rate, and no $CH_3O_2NO_2$ chemistry
MPN case	Sander et al. [*Sander et al.*, 2011] recommended gas-phase rate constants, Evans and Jacob[*Evans and Jacob*, 2005] recommended N_2O_5 hydrolysis rate, and $CH_3O_2NO_2$ chemistry [*Browne et al.*, 2011; *Nault et al.*, 2015]
PNA case	Sander et al. [*Sander et al.*, 2011] recommended gas-phase rate constants except for reaction rate constant for the reaction of HO_2 with NO_2 to produce HO_2NO_2, [*Bacak et al.*, 2011; *Nault et al.*, 2016] Evans and Jacob [*Evans and Jacob*, 2005] recommended N_2O_5 hydrolysis rate, and no $CH_3O_2NO_2$ chemistry
N_2O_5 case	Sander et al. [*Sander et al.*, 2011] recommended gas-phase rate constants, Evans and Jacob [*Evans and Jacob*, 2005] recommended N_2O_5 hydrolysis rate reduced by a factor of 10 [*Brown et al.*, 2009], and no $CH_3O_2NO_2$ chemistry
HNO_3 case	Sander et al. [*Sander et al.*, 2011] recommended gas-phase rate constants except for reaction rate constant for the reaction of OH with NO_2 to produce HNO_3, [*Henderson et al.*, 2012; *Nault et al.*, 2016] Evans and Jacob [*Evans and Jacob*, 2005] recommended N_2O_5 hydrolysis rate, and no $CH_3O_2NO_2$ chemistry
Updated case	Combines MPN, PNA, N_2O_5, and HNO_3 case
Updated +33% case	Updated case with 33% increase in lightning NO_x emission rates

Supplemental Table 2. Regions used for satellite comparisons in Figure 2 and the months the values are compared.

Region	Longitude	Latitude	Months Investigated
South America	77 – 39°W	35°S – 10°N	DJF
Northern Africa	15°W – 48°E	3 – 25°N	JJA
Southern Africa	10 – 48°E	30°S – 3°N	DJF
Southeast Asia	95 – 146°E	9°S – 26°N	JJA

Supplemental Table 3. Comparison of GEOS-Chem Simulation Results-to-DC3 Observations using different NO_x/HNO_3 ratios for the Base, Updated, and Updated +33% Simulations, defined in Supplemental Table 1. The ratios in the header are the NO_x/HNO_3 ratio used to filter the DC3 observations; the ratios in the table body are the average ratio of modeled NO_x or HNO_3 to the observed quantities.

Species	**Base, Ratio < 5**	**Base, Ratio < 10**	**Base, All Data**	**Updated, Ratio < 5**	**Updated, Ratio < 10**	**Updated, All Data**	**Updated + 33%, Ratio < 5**	**Updated + 33%, Ratio < 10**	**Updated + 33%, All Data**
NO_x	0.80	0.83	0.72	0.79	0.78	0.70	0.98	1.03	0.98
HNO_3	1.48	1.73	2.25	1.33	1.33	1.91	1.59	1.85	2.45

Supplemental Table 4. Comparison of mol NO flash^{-1} and TgN yr^{-1} from this study and other studies.

Study	**mol NO flash^{-1}**	**TgN yr^{-1}**
This Study, Mid-latitude, Model	665	9[a]
This Study, Tropics, Model	346	
This Study, Mid-latitude, Prior Near-field Studies Corrected for Chemistry	550	9 – 10
This Study, Tropics, Prior Near-field Studies Corrected for Chemistry	510	9 – 10
This Study, Tropics, Using NO_y	400 – 479	7 – 9
Average Near-field, Mid-latitude[b]	238	~5
Average Near-field, Tropics[c]	215	~5
Hudman et al. [2007]	500	5.8
Martin et al. [2007]	260	6
Ott et al. [2010]	500	8.6
Jourdain et al. [2010]	520	8
Miyazaki et al. [2014]	310	6.3
Liaskos et al. [2015]	246	5

[a]This 9 TgN yr^{-1} is derived from the GEOS-Chem model run with 665 mol NO flash^{-1} in the midlatitudes and 346 mol NO flash^{-1} in the tropics.

[b]Average from values reported in Schumann and Huntrieser [2007] and Huntrieser [2009].

[c]Average from values reported in Schumann and Huntrieser [2007].

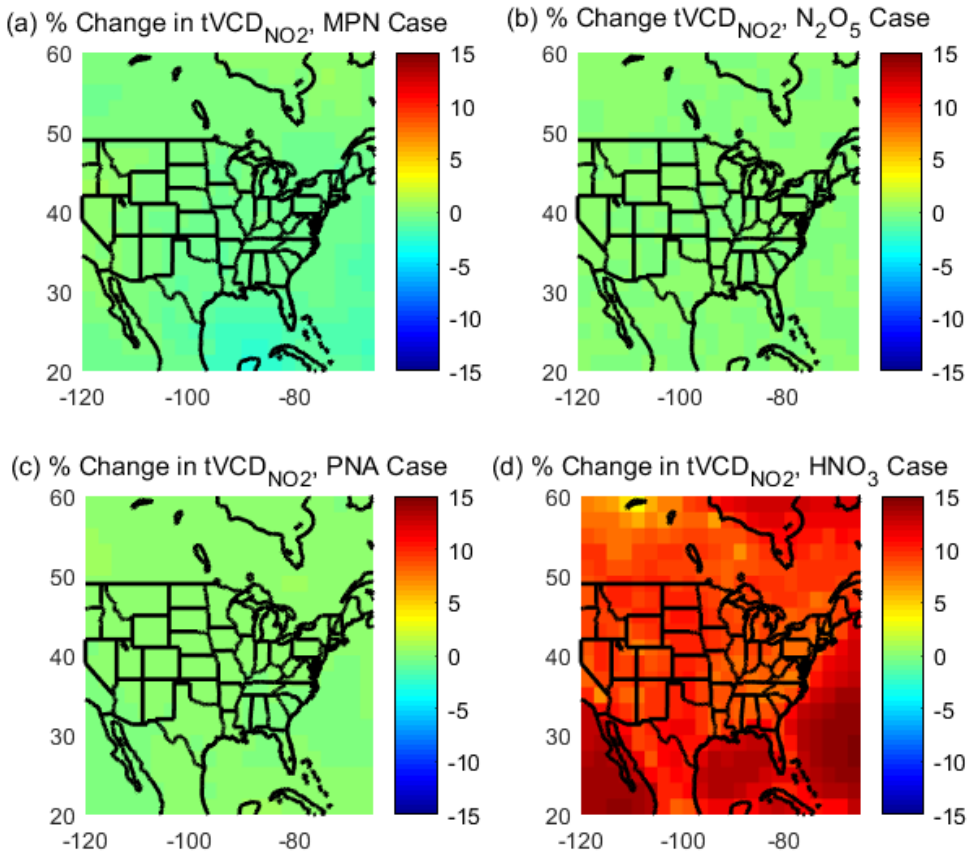

Supplemental Figure 1. Percent changes of average modeled $tVCD_{NO2}$ between Base case and various chemical cases defined in Supplemental Table 1. The average modeled values are for May – June, 2012 for times between 12:00 – 14:00 local time.

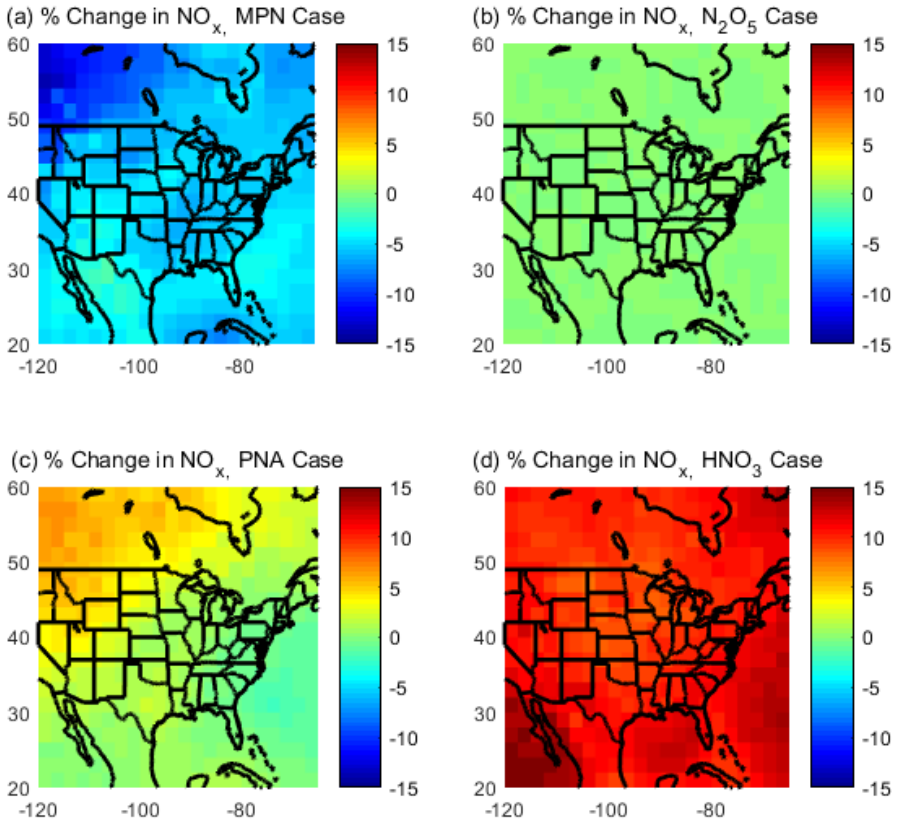

Supplemental Figure 2. Percent changes of average modeled UT (200 – 350 hPa) NO_x between Base case and various chemical cases defined in Supplemental Table 1. The average modeled values are for May – June, 2012 for times between 16:00 – 20:00 local time.

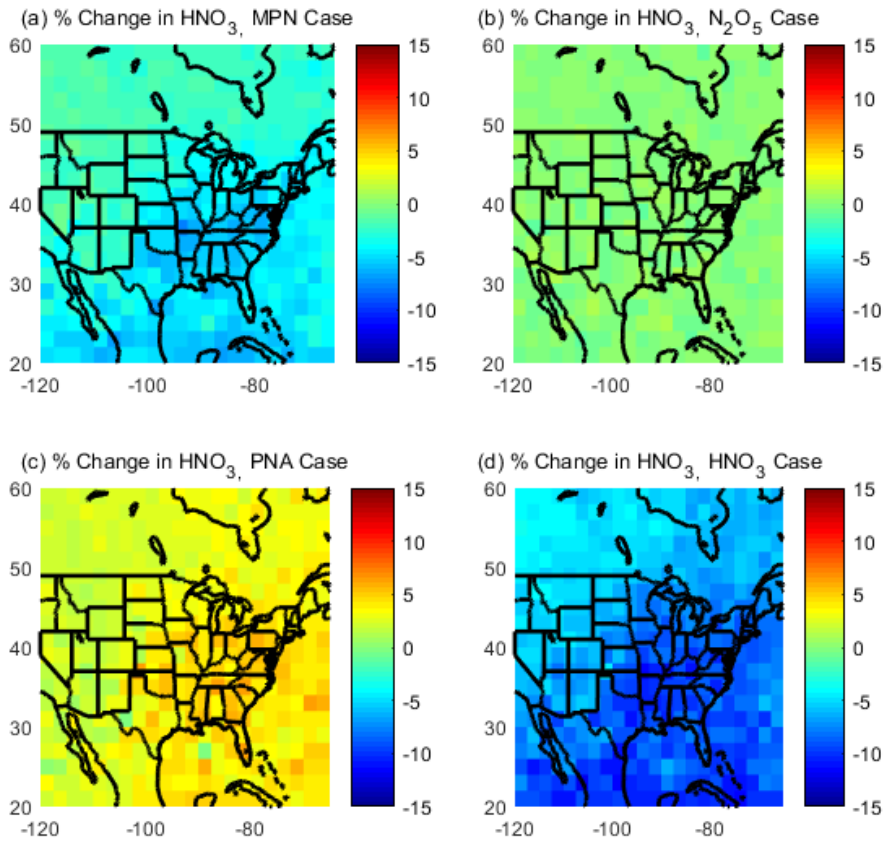

Supplemental Figure 3. Percent changes of average modeled UT (200 – 350 hPa) HNO_3 between Base case and various chemical cases defined in Supplemental Table 1. The average modeled values are for May – June, 2012 for times between 16:00 – 20:00 local time.

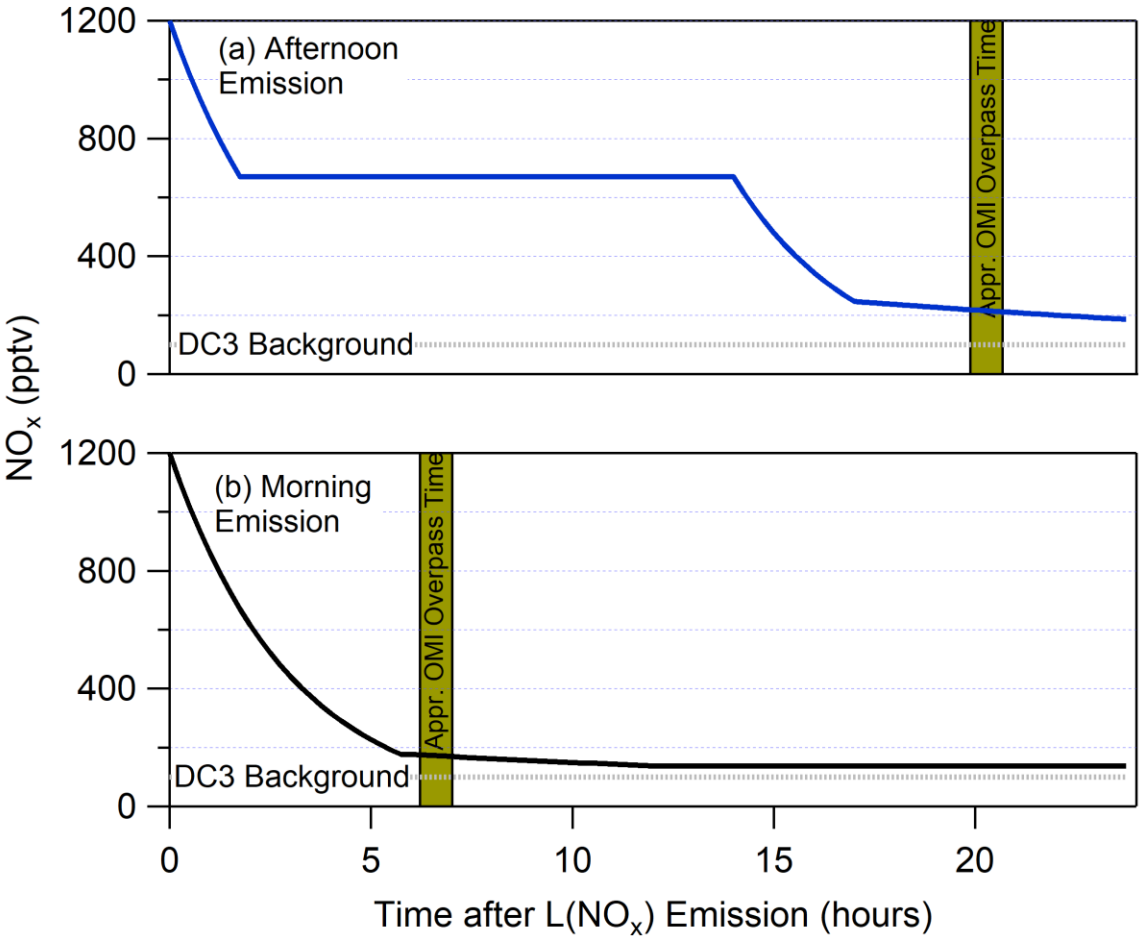

Supplemental Figure 4. (a) Time series of the decay of lightning NO_x, assuming a 17:00 local time emission, and **(b)** time series of the decay of lightning NO_x, assuming a 07:00 local time emission. The vertical gold bars represent the approximate OMI overpass time at ~13:40 local time. The grey dashed line represents the average DC3 UT NO_x background of ~100 pptv [*Barth et al.*, 2015].

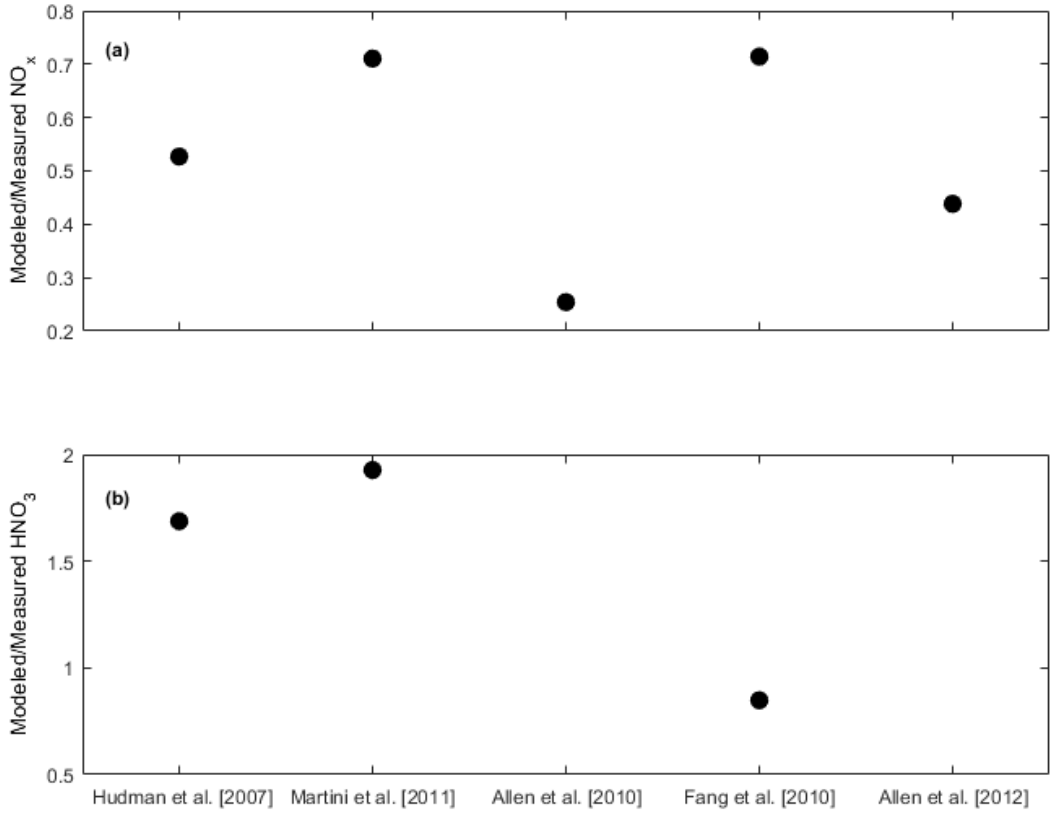

Supplemental Figure 5. (a) Ratio of modeled and measured UT NO_x from Hudman et al. [2007], Martini et al. [2011], Allen et al. [2010], Fang et al. [2010], and Allen et al. [2012] The NO_x values are corrected as suggested by Browne et al. [2011] (b) Ratio of modeled and measured UT HNO_3 from Hudman et al. [2007], Martini et al. [2011], and Fang et al. [2010] The HNO_3 values are corrected as suggested by Bertram et al. [2007]

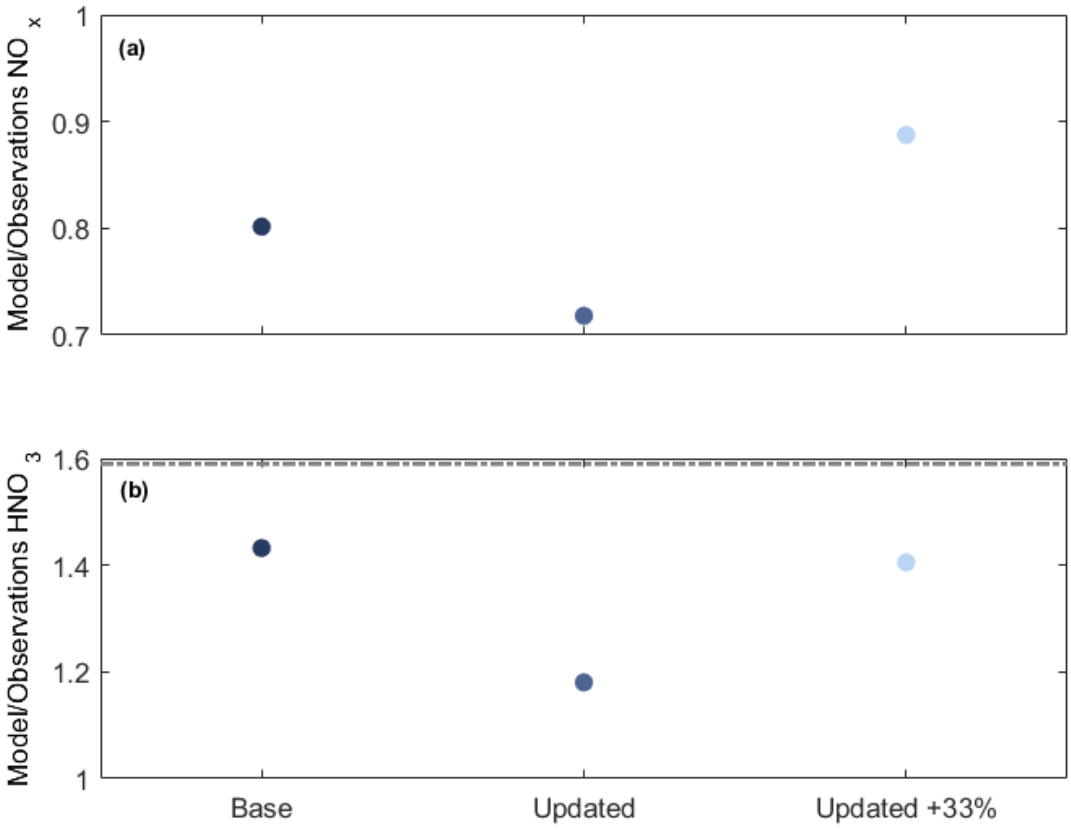

Supplemental Figure 6. Same as Figure 2, but correcting the updated values with the amount of ANs produced downwind of deep convection by 30 pptv [*Nault et al.*, 2016]. The grey dashed-dot line represents the upper 1σ limit of observations during DC3, similar to Figure 1.

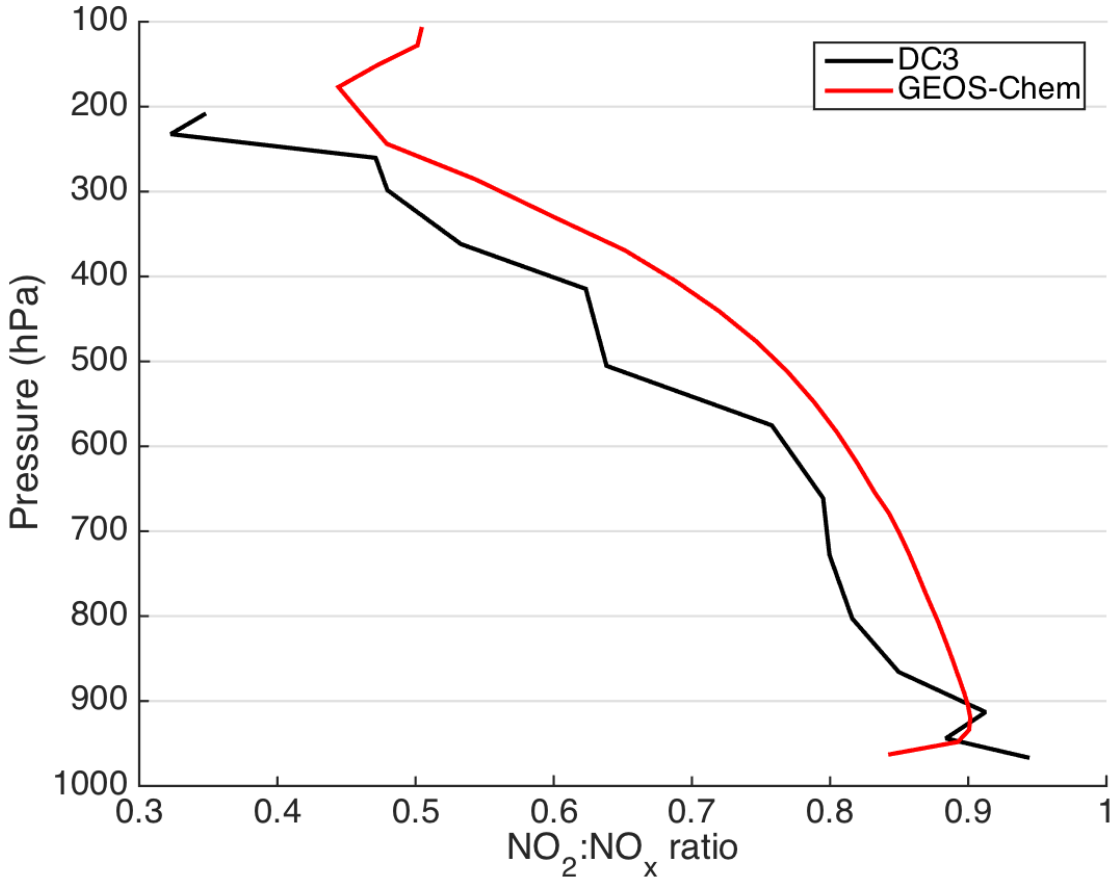

Supplemental Figure 7. NO_2:NO_x ratios averaged over the DC3 campaign and GEOS-Chem grid cells matching the DC3 domain.

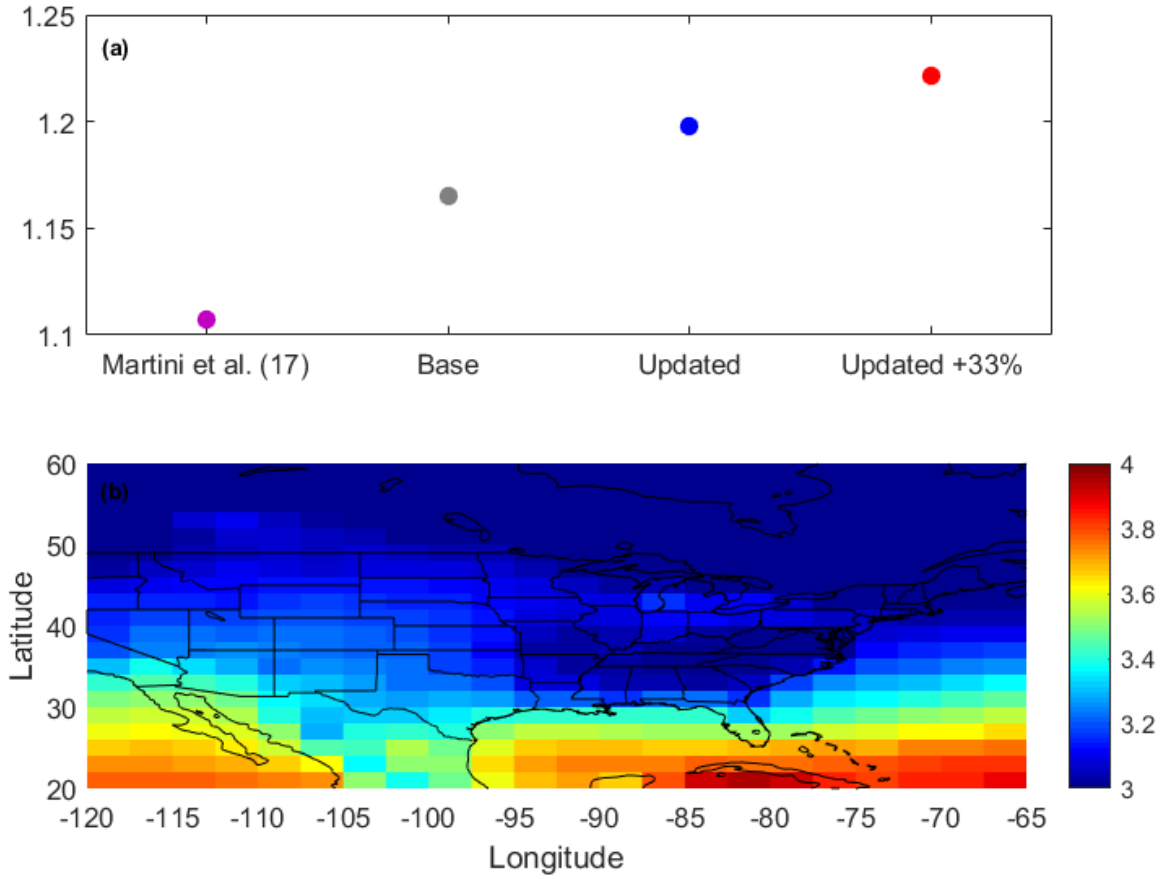

Supplemental Figure 8. (a) Ratio of modeled and observed O_3 from Martini et al.[Martini et al., 2011] and from DC3 with Base case, Updated case, and Updated +33% case. (b) Percent changes of average modeled UT (200 – 350 hPa) O_3 mixing ratios (pptv) between Base case and Updated case, defined in Supplemental Table 1. The average modeled values are for May – June, 2012.

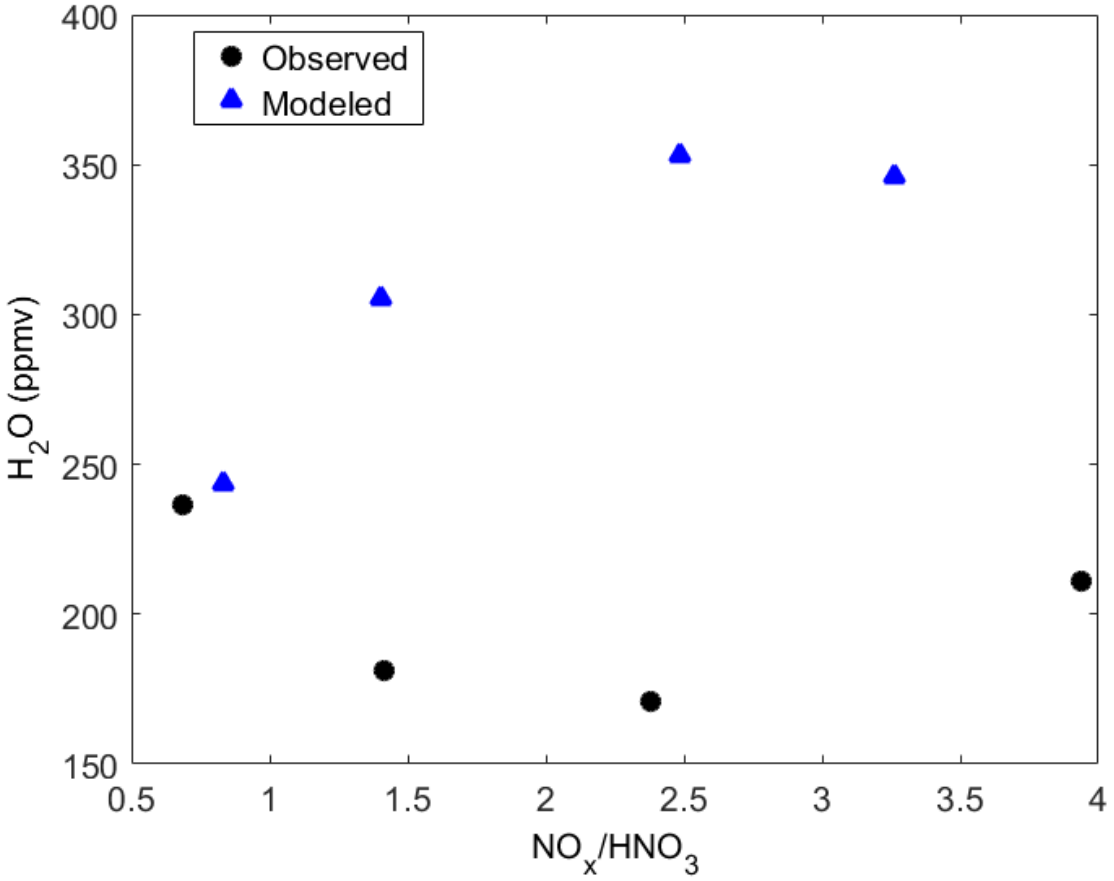

Supplemental Figure 9. Comparison of modeled (blue) and observed (black) UT water vapor during DC3 versus chemical age (NO_x/HNO_3) since convection [*Bertram et al.*, 2007]

Allen, D., K. Pickering, B. Duncan, and M. Damon (2010), Impact of lightning NO emissions on North American photochemistry as determined using the Global Modeling Initiative (GMI) model, *J. Geophys. Res.*, *115*, doi:doi:10.1029/2010JD014062.

Allen, D. J., K. E. Pickering, R. W. Pinder, B. H. Henderson, K. W. Appel, and A. Prados (2012), Impact of lightning-NO on eastern United States photochemistry during the summer of 2006 as determined using the CMAQ model, *Atmos. Chem. Phys.*, *12*(4), 1737–1758, doi:doi:10.5194/acp-12-1737-2012.

Archive, National Aeronautical and Space Agency, Deep Convective Clouds and Chemistry, DC-8, Version 5, *2014*(September 20). Available from: 10.5067/Aircraft/DC3/DC8/Aerosol-TraceGas

Bacak, A. et al. (2011), Kinetics of the HO_2 + NO_2 Reaction: On the impact of new gas-phase kinetic data for the formation of HO_2NO_2 on HO_x, NO_x and HO_2NO_2 levels in the troposphere, *Atmos. Environ.*, *45*(35), 6414–6422, doi:10.1016/j.atmosenv.2011.08.008.

Barth, M. C. et al. (2015), The Deep Convective Clouds and Chemistry (DC3) Field Campaign , *Bull. Am. Meteorol. Soc.*, *96*(8), 1281–1309, doi:10.1175/BAMS-D-13-00290.1.

Bertram, T. H. et al. (2007), Direct Measurements of the Convective Recycling of the Upper Troposphere, *Science (80).*, *315*(5813), 816–820, doi:10.1126/science.1134548.

Boersma, K. F., E. J. Bucsela, E. J. Brinksma, and J. F. Gleason (2002), *NO_2, OMI Algorithm Theor. Basis Doc. Vol. 4, Omi Trace Gas Algorithms, ATB-OMI-04, version 2.0*, 13–36. Available from: http://eospso.nasa.gov/sites/default/files/atbd/ ATBD-OMI-04.pdf (Accessed 22 November 2016).

Boersma, K. F., Braak, R. and R. J. van der A (2011), *Dutch OMI NO_2 (DOMINO) data product 2.0 HE5 data file user manual*, p. 17. Available from http://www.temis.nl/docs/OMI_NO2_HE5_2.0_2011.pdf (Accessed 25 Aug 2017).

Brown, S. S. et al. (2009), Reactive uptake coefficients for N_2O_5 determined from aircraft measurements during the Second Texas Air Quality Study: Comparison to current model parameterizations, *J. Geophys. Res.*, *114*, D00F10, doi:10.1029/2008JD011679.

Browne, E. C. et al. (2011), Global and regional effects of the photochemistry of $CH_3O_2NO_2$: evidence from ARCTAS, *Atmos. Chem. Phys.*, *11*(9), 4209–4219, doi:doi:10.5194/acp-11-4209-2011.

Cooper, M., R. V Martin, C. Wespes, P.-F. Coheur, C. Clerbaux, and L. T. Murray (2014), Tropospheric nitric acid columns from the IASI satellite instrument interpreted with a chemical transport model: Implications for parameterizations of nitric oxide production by lightning, *J. Geophys. Res.*, *119*(16), 10068–10079, doi:10.1002/2014JD021907.

Crounse, J. D., K. A. McKinney, A. J. Kwan, and P. O. Wennberg (2006), Measurement of Gas-Phase Hydroperoxides by Chemical Ionization Mass Spectrometry, *Anal. Chem.*, *78*(19), 6726–6732, doi:doi:10.1021/ac0604235.

Day, D. A., P. J. Wooldridge, M. B. Dillon, J. A. Thornton, and R. C. Cohen (2002), A thermal dissociation laser-induced fluorescence instrument for in situ detection of NO_2, peroxy nitrates, alkyl nitrates, and HNO_3, *J. Geophys. Res.*, *107*(D5-6), 4046, doi:10.1029/2001JD000779.

Diskin, G. S., J. R. Podolske, G. W. Sachse, and T. A. Slate (2002), Open-path airborne tunable diode laser hygrometer, in: Diode Lasers and Applications in Atmospheric Sensing, edited by: Fried, A., *Proc. Soc. Photo-Optical Instrum. Eng.*, *4817*, 196–204, doi:10.1117/12.453736.

Evans, M. J., and D. J. Jacob (2005), Impact of new laboratory studies of N_2O_5 hydrolysis on

global model budgets of tropospheric nitrogen oxides, ozone, and OH, *Geophys. Res. Lett.*, *32*(9), 1–4, doi:10.1029/2005GL022469.

Fang, Y., A. M. Fiore, L. W. Horowitz, H. Levy , II, Y. Hu, and A. G. Russell (2010), Sensitivity of the NO_y budget over the United States to anthropogenic and lightning NO_x in summer, *J. Geophys. Res.*, *115*, D18312–D18312, doi:10.1029/2010JD014079.

Henderson, B. H. et al. (2011), Evaluation of simulated photochemical partitioning of oxidized nitrogen in the upper troposphere, *Atmos. Chem. Phys.*, *11*(1), 275–291, doi:10.5194/acp-11-275-2011.

Henderson, B. H., R. W. Pinder, J. Crooks, R. C. Cohen, A. G. Carlton, H. O. T. Pye, and W. Vizuete (2012), Combining Bayesian methods and aircraft observations to constrain the HO_2 + NO_2 reaction rate, *Atmos. Chem. Phys.*, *12*(2), 653–667, doi:10.5194/acp-12-653-2012.

Hudman, R. C. et al. (2007), Surface and lightning sources of nitrogen oxides over the United States: Magnitudes, chemical evolution, and outflow, *J. Geophys. Res.*, *112*, D12S05, doi:doi:10.1029/2006JD007912.

Huntrieser, H. et al. (2009), NO_x production by lightning in Hector: first airborne measurements during SCOUT-O3/ACTIVE, *Atmos. Chem. Phys.*, *9*(21), 8377–8412, doi:10.5194/acp-9-8377-2009.

Jourdain, L., S. S. Kulawik, H. M. Worden, K. E. Pickering, J. Worden, and A. M. Thompson (2010), Lightning NO_x emissions over the USA constrained by TES ozone observations and the GEOS-Chem model, *Atmos. Chem. Phys.*, *10*(1), 107–119, doi:10.5194/acp-10-107-2010.

Levelt, P. F., G. H. J. Van den Oord, M. R. Dobber, A. Malkki, H. Visser, J. de Vries, P. Stammes, J. O. V Lundell, and H. Saari (2006), The Ozone Monitoring Instrument, *IEEE Trans. Geosci. Remote Sens.*, *44*(5), 1093–1101, doi:10.1109/TGRS.2006.872333.

Liaskos, C. E., D. J. Allen, and K. E. Pickering (2015), Sensitivity of tropical tropospheric composition to lightning NO_x production as determined by replay simulations with GEOS-5, *J. Geophys. Res. Atmos.*, doi:10.1002/2014JD022987.

Martin, R. V, B. Sauvage, I. Folkins, C. E. Sioris, C. Boone, P. Bernath, and J. Ziemke (2007), Space-based constraints on the production of nitric oxide by lightning, *J. Geophys. Res. Atmos.*, *112*(D9), D09309–D09309, doi:10.1029/2006JD007831.

Martini, M., D. J. Allen, K. E. Pickering, G. L. Stenchikov, A. Richter, E. J. Hyer, and C. P. Loughner (2011), The impact of North American anthropogenic emissions and lightning on long-range transport of trace gases and their export from the continent during summers 2002 and 2004, *J. Geophys. Res. Atmos.*, *116*, D07305–D07305, doi:10.1029/2010JD014305.

Miyazaki, K., H. J. Eskes, K. Sudo, and C. Zhang (2014), Global lightning NO_x production estimated by an assimilation of multiple satellite data sets, *Atmos. Chem. Phys.*, *14*(7), 3277–3305, doi:10.5194/acp-14-3277-2014.

Nault, B. A., C. Garland, S. E. Pusede, P. J. Wooldridge, K. Ullmann, S. R. Hall, and R. C. Cohen (2015), Measurements of $CH_3O_2NO_2$ in the upper troposphere, *Atmos. Meas. Tech.*, *8*(2), 987–997, doi:10.5194/amt-8-987-2015.

Nault, B. A. et al. (2016), Observational Constraints on the Oxidation of NOx in the Upper Troposphere, *J. Phys. Chem. A*, *120(9)*, 1468–1478, doi:10.1021/acs.jpca.5b07824.

Ott, L. E., K. E. Pickering, G. L. Stenchikov, D. J. Allen, A. J. DeCaria, B. Ridley, R.-F. Lin, S. Lang, and W.-K. Tao (2010), Production of lightning NO_x and its vertical distribution calculated from three-dimensional cloud-scale chemical transport model simulations, *J.*

Geophys. Res., *115*, D04301–D04301, doi:10.1029/2009JD011880.

Pollack, I. B. et al. (2016), Airborne quantification of upper tropospheric NO_x production from lightning in deep convective storms over the United States Great Plains, *J. Geophys. Res. Atmos.*, *121*(4), 2002–2028, doi:10.1002/2015JD023941.

Ryerson, T. B., L. G. Huey, K. Knapp, J. A. Neuman, D. D. Parrish, D. T. Sueper, and F. C. Fehsenfeld (1999), Design and initial characterization of an inlet for gas-phase NO_y measurements from aircraft, *J. Geophys. Res.*, *104*(D5), 5483–5492, doi:doi:10.1029/1998JD100087.

Sander, S. P. et al. (2011), Chemical Kinetics and Photochemical Data for Use in Atmospheric Studies, Evaluation No. 17, *JPL Publ. 10-6, Jet Propuls. Lab. Pasadena*.

Schumann, U., and H. Huntrieser (2007), The global lightning-induced nitrogen oxides source, *Atmos. Chem. Phys.*, *7*(14), 3823–3907, doi:10.5194/acp-7-3823-2007

Talbot, R. W. et al. (1997), Large-scale distributions of tropospheric nitric, formic, and acetic acids over the western Pacific basin during wintertime, *J. Geophys. Res.*, *102*(D23), 28303–28313, doi:10.1029/96JD02975.

Thornton, J. A., P. J. Wooldridge, and R. C. Cohen (2000), Atmospheric NO_2: In-situ laser-induced fluorescence detection at parts per trillion mixing ratios, *Anal. Chem.*, *72*(3), 528–539, doi:10.1021/ac9908905.